FREE DIRECTIONAL ROBOTIC DEPOSITION - INFLUENCE ON OVERHANG PRINTABILITY

PETR KREJCIRIK, DAVID SKAROUPKA, DAVID PALOUSEK

Brno University of Technology, Faculty of Mechanical Engineering, NETME Centre, Czech Republic

DOI: 10.17973/MMSJ.2018_12_2018119

e-mail: Petr.Krejcirik@vutbr.cz

This article deals with a 3D printing strategy to reduce supports in the case of overhang geometry on 3D printed models realized by Fused Filament Fabrication (FFF). Experiments were performed to compare the conventional FFF process (normal orientation to the platform) with a novel strategy of 3D printing using 6-axis degrees of freedom to orient the nozzle close to the tangent direction of the 3D printed wall. The shape accuracy of the printed specimens was evaluated by an optical 3D scanner and the cross sections of the layers were observed by a digital microscope.

KEYWORDS

3D printing strategy, 6-axis 3D printing, robotic 3D printing, fused filament fabrication, FFF, PLA, spiral vase, KUKA PRC, Grasshopper

1 INTRODUCTION

Currently, there is a rapid increase in fields where the production of prototypes or product is realized by Fused Filament Fabrication (FFF). Thanks to the additive manufacturing principle, there are considerable material savings compared to conventional production (e.g. machining or casting). Since the material is applied to free space (no form is included), this method carries some geometrical or technological limitations. It is necessary to create a basic structure for applying molten material. Without this basic structure, material will flow to the ground due to gravitational action. Ideally, this base structure for the appropriate layer is part of the body. However, it is not always possible to design the component with this condition. In case of overhang printing (e.g. holes or bridges), the structure to which the molten material would be applied is not part of the required model. In this case, it is necessary to create a supporting structure that serves only as a base for the application of the material. Once the print is complete, this structure is removed from the printed part in the post-processing steps. Constructing the support structures means increasing the production time, the economics costs and the time spent on finishing operations with the created body. As a result, production becomes less efficient and more expensive. Conventional 3D printer concepts are implemented with 3 degrees of freedom, ensuring movement along three axes of the XYZ coordinate system. The KUKA KR 60 HA robotic arm is equipped with 6 degrees of freedom, which allows the tool to tilt around all 3 axes of the cartesian coordinate system. Thanks to this, the robotic arm can be used, for example, to match more complex parts that need to be machined from several directions. This makes production more efficient, as it is not necessary to turn and re-fix the workpiece for several machining planes. In 3D printing applications, it is possible to apply molten material by tilting the print head. Due to the change in the direction of material deposition, there is a geometry change of the printed layer with a better contact area, which can result in far larger overhangs without the use of support structures compared to the classic 3D printer concept. Another advantage of the robotic workplace is larger workspace, making it possible to produce larger pieces.

Jiang et al.[Jiang 2018] examined the influence of the process parts on the printable threshold of the overhang angle. For the experiment was used the PLA material in form of 1.75 mm filament diameter. Extrusion temperature was investigated in the range of 175 – 220 °C. The results show that with the increasing extrusion temperature there is a rise of the mean deformation at the printed parts. The mean deformation of the overhang section also rises with faster material deposition. Cooling of the deposited material provides a minimal decrease of deformation with an increase of the fan speed. Experiments to determine deformation dependent on the overhang angle were realized with these tuned process parameters. Results of these experiments show a rapid rise of the deformation when the angle between the wall and the build plate decreases.

Bellehumer et al. [Bellehumer 2004] described the bond formation between deposited layers. A bond can be realized in three different modes – surface contact, neck growth and diffusion at the interface of the deposited layers. Surface contact can be observed when the distance between the center of the deposited layers is equivalent to the layer dimension. If the distance is lower, a bond surface is created between deposited layers. If the temperature of both connected layers is higher than glass transition temperature (T_g), a diffusion at the layer interface appears. However, if the temperature is lower than T_g, a cold bond is created without diffusing layer interface. In this case, the interface of the layers has a shape with contact surface that is less wide than the layer width. This type of interface is called neck growth. Compared to the diffusion interface, the bond has lower strength.

Sun et al. [Sun 2008] studied the influence of the FFF processing parameters on the bonding quality between the deposited layers. The quality of bond was evaluated by monitoring the width of the neck formed between layers. They concluded that the temperature inside chamber and the heat convection through the printed samples have a significant effect on the bond quality and the shear strength between two bonded layers.

Li et al. [Li 2018] developed the heat transfer numerical model of the bond formation between deposited layers. This model describes the cooling of the material after the extrusion through the nozzle and the neck width in the bond between deposited layers. The conclusion of the paper is that the material is cooled below the glass transition temperature (T_g) too fast to be able to carry another layer of material. Material deposition at a temperature under the T_g means that there is no diffusion between deposited layers. This causes lower bond strength than the tensile strength of the layer.

Coogan et al. [Coogan 2017] compared bond and part strength of FFF specimens build with different process parameters – nozzle temperature, print speed, fibre width, layer height and fibre deposit orientation. Bond strength of the specimens increases rapidly with higher deposited fibre width and lower layer height. A smaller increase can be observed with higher print speed and nozzle temperature. The temperature of the platform has minimal effect on the bond strength.

For printing product with large dimensions, it is appropriate to minimize build time and material consumption while maintaining the required accuracy. With this task is offered increasing the diameter of the nozzle with which a higher volume flow of the molten material can be reached. Results from Coogan et al. [Coogan 2017] show that increasing the

volume flow of the material has a positive effect on the strength of the bond between the deposited layers. With this conclusion some types of shapes could be printed as a one-path shell without an infill structure.

With the research conclusion [Coogan 2017] it is suitable to apply material in lower layer height, higher layer width and with higher printing speed for gaining a better result in bond strength.

Zhao et al. [ZHAO, 2018] developed the new printing strategy with inclined layer printing. Printed parts with overhang areas are split into groups by overhang angle. These groups are sliced with relative angle to the build plate according to overhang angle. Change of the toolpath at the overhang provides a better bond between the deposited layers, resulting in higher overhang angle printing without using support structures.

Herrmann and Tolar [Herrmann 2016] developed a 6-axis 3D printer. Both the print head and the build plate have the possibility to move and rotate in all 6 Degrees of Freedom in Cartesian system. This offers the opportunity to print overhang sections by tilting the print head or build. When tilting the build plate, the angle between the overhang angle and the gravitational action can be decreased. However, the 3D printer does not have the synchronous control of the build plate and the print head, which significantly reduces the possibilities of this machine.

2 MATERIAL AND METHODS

Research was realized by a 3D printing system with a customized print head mounted to the KUKA KR 60 HA 6-axis robotic arm. Evaluation of the results was provided using ATOS Triple scanoptical scanner, Olympus SZX7 microscope and GOM Inspect and Rhinoceros software.

2.1 *Methodology pipeline*

The basic methodology can be described as follows:

1. Design– geometry of the specimen
2. Scripting – 3D printing strategy
3. Trajectories – movement code generation
4. Experiments – Robotic 3D printing
5. Evaluation –shape accuracy and cross-sections

2.2 *Kuka KR 60 HA*

KUKA KR 60 HA is a 6-axis robotic arm manufactured by KUKA AG. Parameters of the machine are presented in Table 1.

Parameter	Value
Rated payload	60 kg
Maximum reach	2033 mm
Pose repeatability	± 0.05 mm
Controller	KR C2

Table 1. KUKA KR 60 HA parameters

The trajectory of the robotic arm end effector is generated in Grasshopper KUKA PRC software which is an extension to the Rhinoceros (McNeel Europe) CAD software. A special algorithm creates the code in KRL (KUKA Robot Language) which describes the movement and orientation of the end effector through the generated path. This code is transferred to the KUKA Robotic controller.

2.3 *Print Head*

Deposition of the molten material is realized by a customized print head. Material is extruded through a nozzle with a 2 mm diameter. The nozzle and the heat block are realized as one piece in order to minimize the peak angle of the nozzle. This is necessary for tilting the print head without a risk of collision with the build plate. The nozzle is connected to the heat break and the mechanism guiding plastic filament to the nozzle. Print head electronic parts: stepper, heating element and thermistor, are controlled by Arduino MEGA 2560microcontroller.

Deposited material is cooled by flowing air from distribution of pressure air in the plant. Air is directed to the printed part through the pneumatic pressure regulator, operating valve and customized blowing nozzles with a 4 mm inner diameter. The pneumatic pressure regulator allows continuous controlling of the flow rate of the compressed air.

2.4 *Printed Materials*

Experiments are designed for open environment with a temperature of 21°C. Therefore, it is better to select a material with a low value of the shrinkage factor to avoid common 3D printing failures caused by a higher heat gradient.Other parameters for the material selection are sufficient viscosity and maximal tensile strength. Table 2 [Stratasys 2018] shows a comparison of the basic materials used in 3D FFF printing applications, where PLA (Polylactic Acid) is closest to the preferred criteria.

Material	PLA	ABS	PET-G
Shrinkage [10^{-6} K^{-1}]	55	73.8	70
Tensile Strength [MPa]	65	90	53
Glass transition temperature [°C]	68	85	70
Viscous flow temperature [°C]	210	230	260
Melt Flow Index [g/10 min]	6-78	1-36	4-15

Table 2. Material properties for basic 3D FFF printing materials

The stock material isused in form of a PLA filament with a 2.85 mm diameter.

2.5 *3DPrinting Strategy*

The core idea how to tackle building-up overhangs without support material is our **hypothesis of self-supportivefibre deposition**. We assume that if the fibre deposition is wall direction informed, then every new layer is supported by the previous one due to eliminating high stepovers, typical for conventional 3D printing strategy. We also assume that capillary forces in the molted material will be higher than gravitation forces to prevent material from sagging.

To incorporate this idea into the 3D printing strategy, we have developed a script in Grasshopper. It is based on the “spiral vase” strategy, but it has been utilized for tilting the printhead (and therefore direction of the fibre deposition) during 3D printing. Tilting was performed to the tangent direction of the wall, as close as robot kinematic allows. The reference value of the maximum overhang angle printed without supporting structures and the influence of the tilt of the printhead was determined experimentally (Figure 1).

For the robotic FFF experiment were tuned process parameters described in Table 3.

Parameter	Value
Layer height	1 mm
Stepper speed	3 rpm
End-effector speed	0.15 m/s
Nozzle temperature	195 °C
Air input pressure	0.02 MPa

Table 3. 3D FFF printing process parameters used in the experiments

Figure 1. Tilting the print head in direction of the tangent surface

The shape of the printed specimens was designed as a conical shell with an increasing overhang angle. The cross-section of the specimens is circular due to elimination of the sharp edge effects. Dimensions of the specimen's shape are displayed in Figure 2.

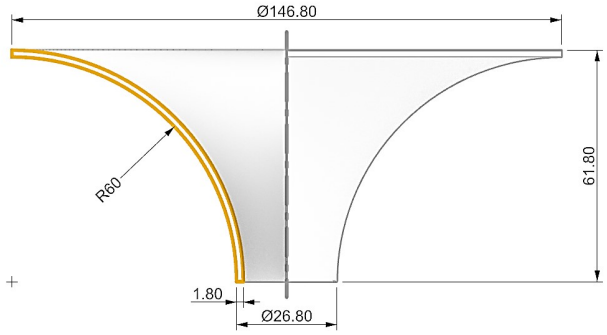

Figure 2. Specimen dimensions and shape

The printed shape was designed to investigate the ability to deposit material to the overhang section without a supporting structure. The overhang angle of the designed shell gradually increases from 0° to 90° between normal of build plate and the normal of the shell element.

To simulate an overhang angle wider than 90°, there is a modification of the build plate orientation. Normally, bodies are printed to the build plate placed at the horizontal orientation (XY plane of the global coordinate system) with normal direction +Z. Research of the ability to create an overhang in the range from 90° to 180° referenced to the global Z axis, build plate was oriented to the plane parallel to global XZ plane and normal vector in direction of negative global vector Y. Experimental 3D printing set-up is displayed in Figure 3

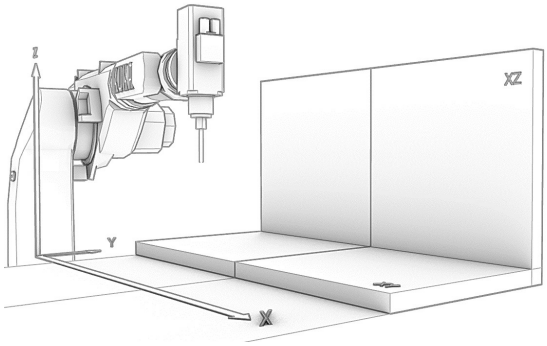

Figure 3. Experimental robotic 3D printing set-up

Trajectory of the robotic arm end effector is calculated in Grasshopper software. The input data is a CAD model of the shell part. A customized slicer places the body to the print build plate with the specified cartesian coordinates. The slicer provides automatic generating of the tool path with defined process parameters (e.g. layer height, control points distance, end-effector speed). The tilting of the printhead is dependent on the shape of the body. Because of the kinematic limits of the 6-axis robotic arm, it is not possible to cover the whole 180° angle as you can see in Figure 4. Therefore, there is a limitation in tilting angle to secure the printing operation without a threat of collision.

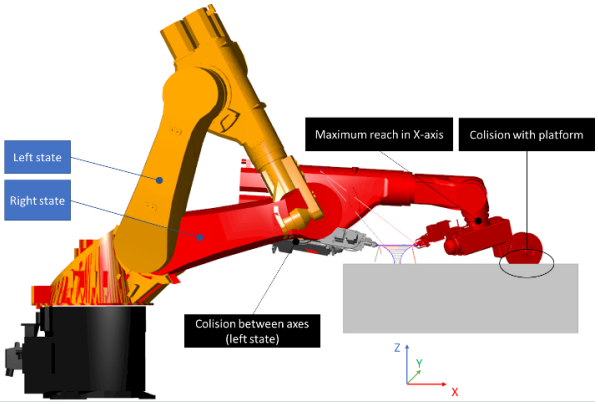

Figure 4. Kinematic limits of the print head tilting

To maximize velocity interpolation, there is analgorithm that computed the ideal printhead orientation in each of the path nodes. The computed trajectory is transferred to the KUKA Robot Language by using the KUKA|prcplugin.

2.6 *Geometric Accuracy of the Specimens*

Geometric accuracy of the printed specimens was evaluated by using ATOS Triple Scanoptical scanner. The accuracy of the 3D scanneris set according to ''VDI/VDE 2634, Part 3 Optical 3D-measuring systems, multiple view systems based on area scanning''. The description of the Atos 3D scanning software was presented by presented [Palousek, 2015].

Parameter	Value
Camera pixels [Mpx]	2 x 8
Measuring volume [mm]	170 x 130 x 130
Measuring distance [mm]	490
Lamp	LED
Focal length camera lenses [mm]	40
Focal length projector lens [mm]	60
Point distance [mm]	0.055
Reference points [mm]	Ø 0.8
Camera position	SO

Table 4. ATOS Triple Scan parameters.

The surfaces of the parts were matted using MR 2000 Anti-Reflex Lchalk spray. This ensures better optical conditions with less reflection of the light from the observed material. Scanning of the parts was done using a rotary table which provides 2-axis rotary movement. Evaluation principle of the deviations measurement between the CAD model and scanned data is displayed in Figure 5.

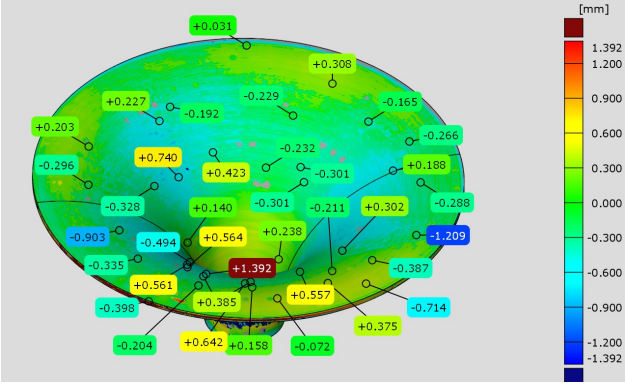

Figure 5. Evaluation of the deviations between CAD model and scanned data

2.7 *Fibre deposition Bond Quality*

The samples were also evaluated for the quality of the bonds between the individual layers. The results were obtained from polished cuts of the relevant samples, which were observed using the Olympus SZX7 microscope and the CANON EOS 1200D camera. Parameters of the device is displayed in Table 5.

Parameter	Value
Effective pixels [Mpx]	18
Aspect ratio	3:2
Low pass filter	Built-in/Fixed
Eyepoint [mm]	21
Magnification	0.80
Resolution	5184x3456
Microscope magnification	51x

Table 5. CANON EOS 1200D parameters

Photos of each segment were merged into a single image. Evaluation of the surface quality and bond contacts were graphically executed in Rhinoceros. The investigation was focused on the fibre width, neck width, and deposited fibre orientation. Measurements were done in each fibre of the examined segments.

3 EXPERIMENTS AND RESULTS

3.1 *3D Printing of Specimens*

Experiments were designed with two major parameters:

a) Orientation of the printhead in relation to the printed part
b) Orientation of the build plate in relation of the gravitational action

With these parameters, 4 types of the specimens were printed (shown in Figure 6). Overview of the printing strategies is displayed in Table 6. Process parameters of the 3D printing were described in chapter 2.5.

Specimens were printed with the same process parameters and environmental conditions. Their evaluation follows three aspects:

1. **Printability (robotic 3D printing)**
2. **Geometric accuracy (optical digitization)**
3. **Fibre deposition bond quality (cross-section cuts)**

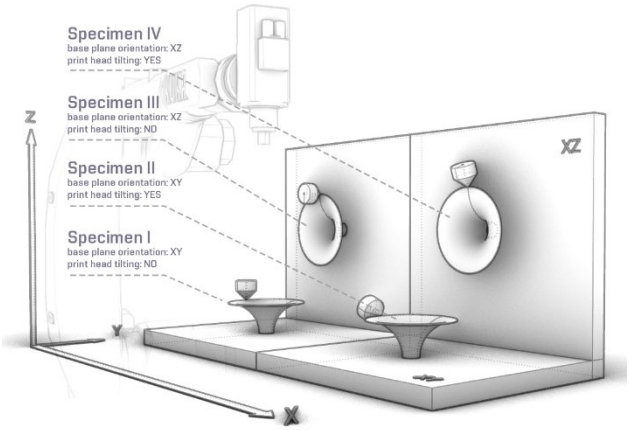

Figure 6. Placement of specimens in the build volume

Specimens	Printhead orientation	Build plate orientation
I	No tilting	Global XY plane
II	Tilting	Global XY plane
III	No tilting	Global XZ plane
IV	Tilting	Global XZ plane

Table 6. Overview of the printed specimens

Specimen I was realized to obtain the reference value of the ability to create an overhang section without a support structure (shown in Figure 7). The threshold of the overhang angle without the presence of a deformation or print failure was compared to the conventional concept of 3D FFF printing.

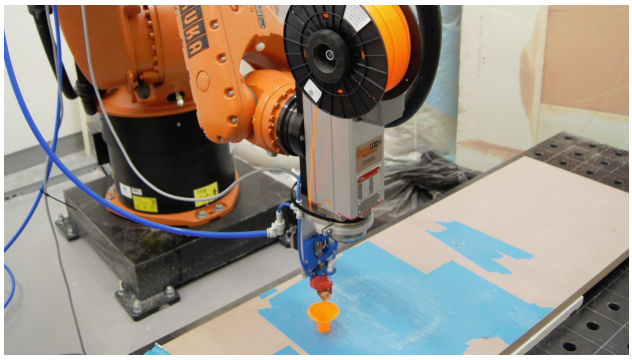

Figure 7. Specimen I printing process

Printing of specimen II was planned with tilting the print head in the direction of the tangent, which was evaluated in each of the trajectory nodes. The printing process with tilting the print head is displayed in Figure 8. However, there is a problem with this task in case of printing larger overhang angles. In this case, the print head needs a large workspace to tilt the print head to the required angle. The dimension of this required space is in the range of several meters and the robotic arm is not capable of performing this task without any collision of robot parts. For that reason, a limitation of the maximal tilt of the printhead referenced to the global Z axis was implemented.

For the experimental printing of specimen II a 38° tilting angle referenced to the global Z axis was assigned.

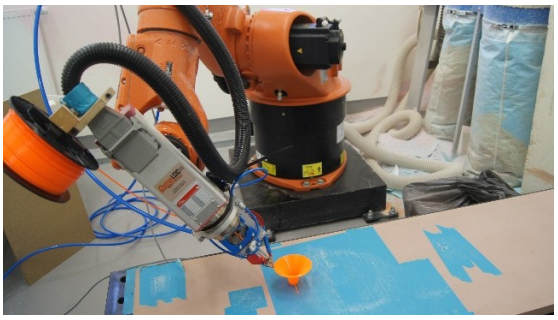

Figure 8. Specimen II printing process

Experiments with specimen I and specimen II provide research of the overhang printing ability without supporting structures in the range of 0° to 90° of the overhang angle. Experiments with specimens III and IV investigate overhang printing ability in the range from 90° to 180° referenced to the global Z vector. This is ensured by modifying the build plate plane from the XY plane to the XZ plane.

Specimen III was realized without tilting the printhead (shown in Figure 9). This experiment serves for comparison and observation of the influence of print head tilting.

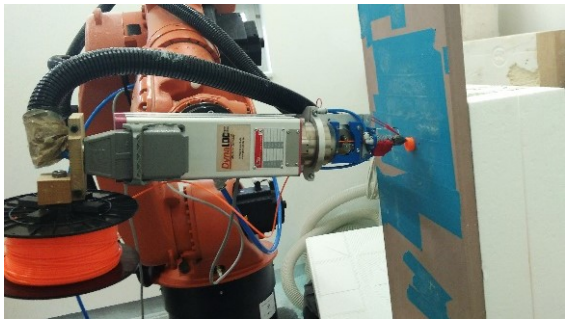

Figure 9. Specimen III printing process

Experiment with specimen IV was realized with tilting the printhead relatively to the normal vector of the build plate (for this configuration of the build plate orientation, the normal vector of the plane is global Y). As with the experiment with specimen II, there is a limitation of the maximum tilting angle due to avoidance of robotic arm parts collision. Maximal tilting angle was set to 38° between tilted printhead and normal vector of the build plate. Tilting of the print head relative to the printed specimen is shown in Figure 10.

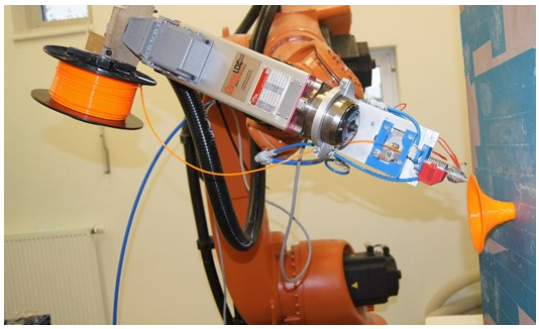

Figure 10. Specimen IV printing process

3.2 Printability – Results

Printability is a familiar expression for the ability of the 3D printing process to build the whole geometry of the part. In this article we evaluate printability from the aspect of ability to build overhang sections).

As shown in Figure 11, printability of the specimens printed with tilting is significantly better than without tilting of the printhead.

We can conclude that the tilting of the printhead during 3D printing process improves the printability of the overhangs. The orientation of the build plate has no significant effect on the capability of building overhang walls, however, there is a visible deviation increase of the geometric accuracy between the evaluated data and the CAD model.

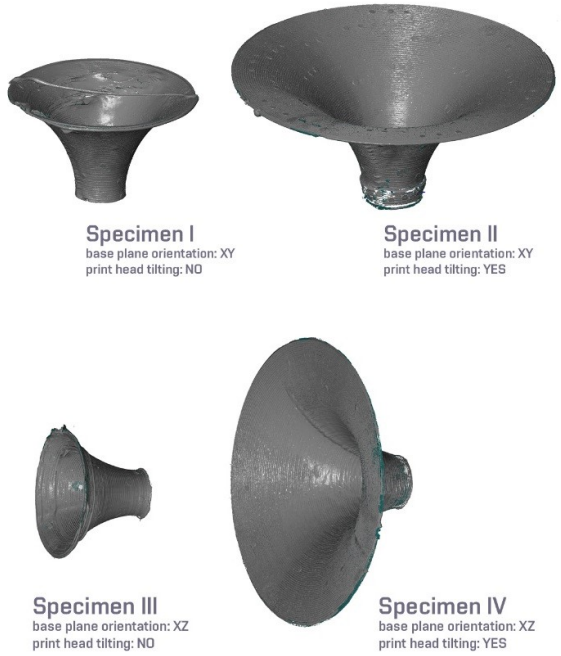

Figure 11. Digitized geometry of the specimens in positions

3.3 Geometric Accuracy – Results

Specimens were digitized optically by the ATOS Triple Scan. Geometric accuracy was evaluated with GOM Inspect software, where digitized specimen geometry was aligned with nominal geometry (conus – CAD model) by gaussian 3-sigma best-fitting method. Deviations were measured, as in the example in Figure 5.

Results of the evaluated geometric accuracy are described in Table 7, showing an influence of platform position and tilting of the printhead on the accuracy of the specimens.

Specim.	Max. Printed overhang angle	Average deviation (mm)	3D Printing finished	Maximal deviation (mm)
I	44°	0.63	NO	1.35
II	90°	0.52	YES	1.39
III	39°	0.61	NO	1.32
IV	90°	0.79	YES	1.75

Table 7. Evaluated printing results from ATOS Triple Scan

Regarding the lower printability of specimens I and III (without tilting), it is possible to compare geometry deviation only with Specimen I to III and Specimen II to IV. These comparisons show effects of the printing on the vertical XZ platform, where the influence of the gravitational action could be expressed. This influence can be described by geometry deviations (Table 7).Specimens I and III are around the same value of the deviation, which leads us to the conclusion that the effect of gravity direction on the fibre deposition (overhang 0°to 44°) is negligible even without tilting. On the contrary, Specimens II

and IV show an increased influence of gravitational forces. Maximal deviation increased by 25% from Specimen II to IV.

3.4 FIBRE DEPOSITION BOND QUALITY – RESULTS

Quality of the interlayer bonds was evaluated as a ratio of the width of the neck between fibres and nominal width of the deposited fibre. These dimensions are marked in Figure 12.

$$k = \frac{b_n}{B} \quad (1)$$

k……bond quality (deposited fibre width ratio)

b_n…… neck width [mm]

B…… Fibre width [mm]

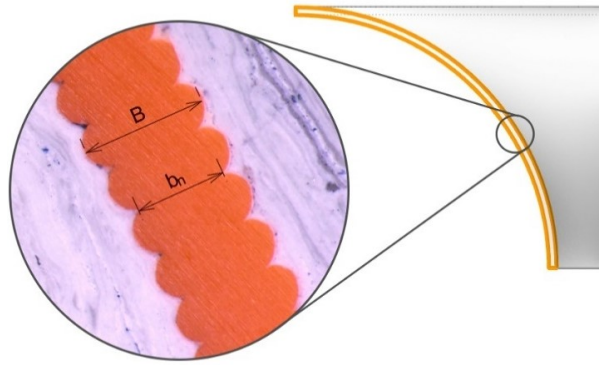

Figure 12. Fibre bond quality measurement

Figure 13 shows acomparison of the 4 printed specimen types with dependency of the fibre bond quality coefficient and sequence of the deposited layers.

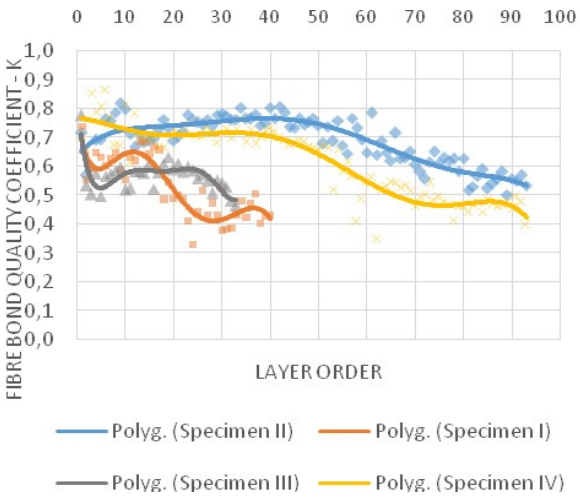

Figure13. Evaluation of the fibre bond quality

The coefficient reaches lowest values in case of the specimens printed without tilting the print head. Specimens printed with tilting the print head achieve a relatively constant course of the value to the overhang of about 40°. **After this, the coefficient value decreases.** It is caused by the limitation of the maximal tilting angle which was set to 38°.

Results show lower values of the coefficient-k calculated at Specimen IV in comparison to the Specimen II. **This means there is an influence of the orientation of the build plate.**

Tilting angle influence was also examined by observing the normal vectors of the bond areas dependent on the sequence of the deposited layers. Normal vectors (shown in Figure 14) were obtained in Rhinoceros software.

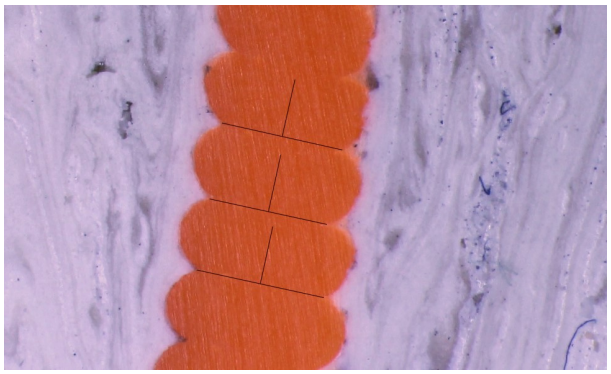

Figure 14.normal vector from the bond area

Figure 15 shows acomparison of the 4 printed specimen types with dependency of the fibre normal vector and sequence of the deposited layers.

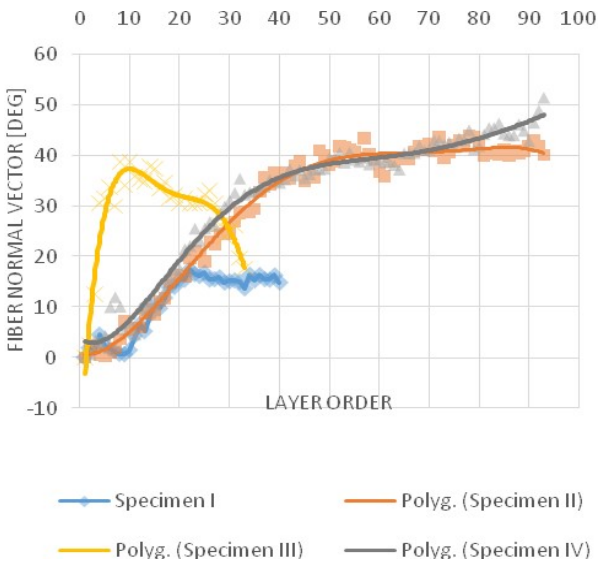

Figure 15. Evaluation of the normal vector from the bond area

Data shows similar results for the fibre vectors measured at specimen II and specimen IV. Deviations of these results can be observed at the end of the part, where the normal vector of specimen IV rises. **This could be caused by gravitational action where the material flows in direction to the ground.**(Figure 16)

Values measured at specimen III support this assumption with showing higher values of the fibre normal vectors than the values gained from Specimen I.

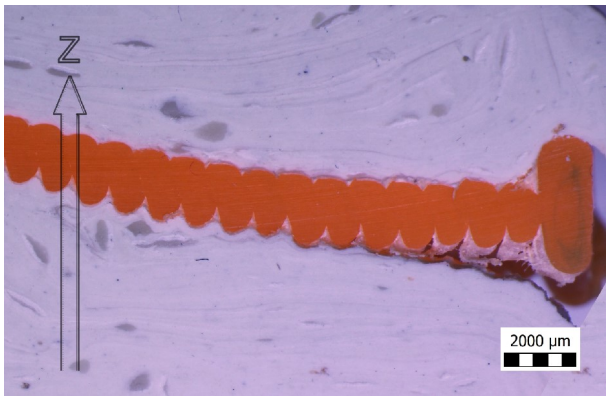

Figure 16. Sagging effect, Specimen III cross-section

4 CONCLUSIONS AND DISCUSSION

Printability (robotic 3D printing)

Four experimental robotic 3D printings were performed. With Specimens I and II on the horizontal XY platform and with specimens III and IV on the vertical XZ platform. On both platforms, printings were tested with and without tilting. Both specimens printed without tilting failed to be printed around 40° overhang (approx. in the middle of shape) and both tilted specimens were printed successfully. We can conclude that printhead tilting to the tangent wall direction increases the printability of higher material overhangs without support.

Geometric accuracy (optical digitization)

Measurements confirm the influence of gravitational action only for overhangs greater than 44°. Specimens II and IV show an increased influence of gravitational forces to the maximum deviation by 25% from Specimen II to IV (both with titling). For better statistical confirmation of this effect more experiments will be performed in the future.

Fibre deposition bond quality (cross-section cuts)

From the successful printability experiments and results described in Figure 12, we can conclude that fibre bond deposition quality is distinctly higher when printhead is tilted. This leads us to the conclusion that the **hypothesis of self-supportive fibre deposition was proved.**

Both specimens are printable on a horizontal XY and vertical XZ platform. Therefore, the influence of the printhead orientation on the printability is much higher than the influence of the gravitational action vector itself. Gravity influences partially shape geometry and the shape of the fibre cross-section, where a partial sagging effect can be visible (Figure 16).The results of our experiments confirm the shape and size of the joint between the fibers studied in [Sun 2008], where with the gradual deposition of the material in the layers the value of the ratio between the width of the neck and the width of the fiber decreases. Sun et al. reached a ratio in the first layers of about 0.61. At the 30rd applied layer was reached a value of the ratio equally 0.41. In our research, ratio values of 0.7 (Specimen II) at the beginning of print and 0.4 (Specimen II) were obtained when the 90 ° overhang was reached. Further research will be focused on a deeper investigation of the Free directional deposition in terms of more complex shapes printability and influence of the bond area normal vector to the geometry accuracy.

Economics aspects

Free Directional Robotic Deposition can create overhang shapes of parts without building support structures. This reduces material and production time costs. Incase of the presented specimens, there is up to 80 % material savings with dependency on the slicer settings. The post-processing is shorter due to absence of the support structure removal operations.

There is a huge potential in term of the workspace size in the robotic 3D printing. Higher purchase prices of 6-axis robotic arms with appropriate accuracy need to be considered. It also affects the right choice of application. We assume that presented 3D printing strategy can be more suitable for the robotized factories or specific operations rather than universal 3D printing system.

ACKNOWLEDGMENTS

This work was supported by NETME Centre, regional R&D centre built with the financial support from the Operational Programme Research and Development for Innovations within the project NETME Centre (New Technologies for Mechanical Engineering),

Reg. No. CZ.1.05/2.1.00/01.0002 and, in the follow-up sustainability stage, supported through NETME CENTRE PLUS (LO1202) by financial means from the Ministry of Education, Youth and Sports under the "National Sustainability Programme I".

REFERENCES

[Bellehumer 2004] Bellehumer, C. et al. Modeling of Bond Formation Between Polymer Filaments in the Fused Deposition Modeling Process, Journal of Manufacturing Processes [online]. 2004, Vol. 6, Issue 2, [cited: 21.10.2018]. Available from: https://doi.org/10.1016/S1526-6125(04)70071-7

[Coogan 2017] Coogan, T. J. et al. Bond and part strength in fused deposition modeling, Rapid Prototyping Journal [online], Vol. 23, Issue: 2, 2017, [cited: 22.10.2018]. Available from: https://doi.org/10.1108/RPJ-03-2016-0050

[Herrmann 2016] Herrmann, D., Tolar, O., ZHAW Master students develop novel 3D printers, ZHAW, 2016, Zurich [online], 3.11.2016, [cited: 16.10.2018]. Available from: https://www.zhaw.ch/de/medien/medienmitteilungen/detailansicht-medienmitteilung/news-single/zhaw-masterstudenten-entwickeln-neuartigen-3d-drucker/

[Jiang 2018] Jiang, J. et al. Investigation of printable threshold overhang angle in extrusion-based additive manufacturing for reducing support waste, International Journal of Computer Integrated Manufacturing [online]. Vol. 31, Issue: 10, 2018, [cited: 20.10.2018]. Available from: https://doi.org/10.1080/0951192X.2018.1466398

[Li 2018] Li, L. et al. Investigation of Bond Formation in FDM Process, SOLID FREEFORM FABRICATION PROCEEDINGS, University of Texas at Austin, 2002, Austin, pp. 400-407 ISSN: 1053-2153

[Palousek 2015] Palousek, D. et al. Effect of matte coating on 3D optical measurement accuracy. *Optical Materials*, February 2015, Vol.40, pp 1-9.ISSN 0925-3467

[Stratasys Ltd. 2018] Stratasys Ltd., What is FDM?: Fused Deposition Modeling Technology for 3D printing – Stratasys, 2018, [cited: 20.10.2018]. Available from: http://www.stratasys.com/fdm-technology

[Sun 2008] Sun, Q. et al. Effect of processing conditions on the bonding quality of FDM polymer filaments, Rapid Prototyping Journal [online], Vol. 14, Issue: 2, 2008, [cited: 16.10.2018]. Available from: https://doi.org/10.1108/13552540810862028

[Zhao 2018] Zhao, H. et al. Inclined layer printing for fused deposition modeling without assisted supporting structure, Robotics and Computer–Integrated Manufacturing [online], Vol. 51, 2018, [cited: 19.10.2018]. Available from: https://doi.org/10.1016/j.rcim.2017.11.011

CONTACT:

Ing. Petr Krejcirik

NETME Centre
Faculty of Mechanical Engineering
Brno University of Technology
Technicka 2896/2, 616 00 Brno, Czech Republic
tel.: +420 541 143 257, e-mail: Petr.Krejcirik@vutbr.cz
http://www.3dlaboratory.cz